Supporting Information

Low-temperature all-vacuum-deposited interfacial layers for high-performance and reproducible flexible inverted organic solar cells and modules

Cheng Shen[1,2], Ze Jin[1,2], Jiaqiang Zhang[1,2], Ran Su[1,2], Yongqi Bai[1], Quan Liu[1,2], Ziyi Ge[1,2*]*

[1] Zhejiang Provincial Engineering Research Center of Energy Optoelectronic Materials and Devices，Ningbo Institute of Materials Technology & Engineering，Chinese Academy of Sciences, Ningbo 315201, China.

[2] Center of Materials Science and Optoelectronics Engineering, University of Chinese Academy of Sciences, Beijing 100049, China

Corresponding authors E-mail: liuquan@nimte.ac.cn, geziyi@nimte.ac.cn.

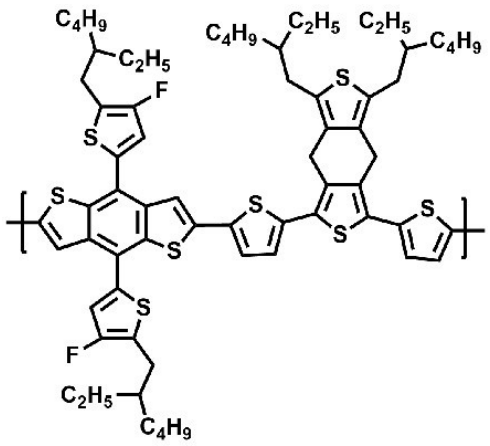

PM6

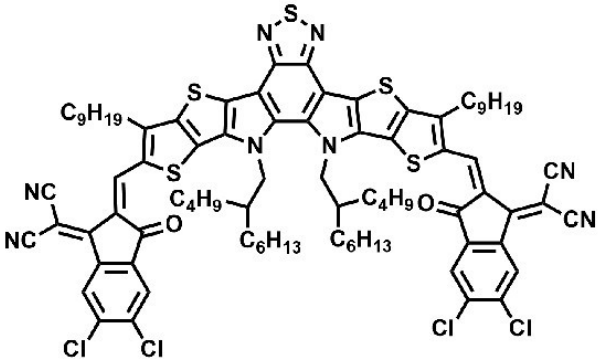

BTP-eC9

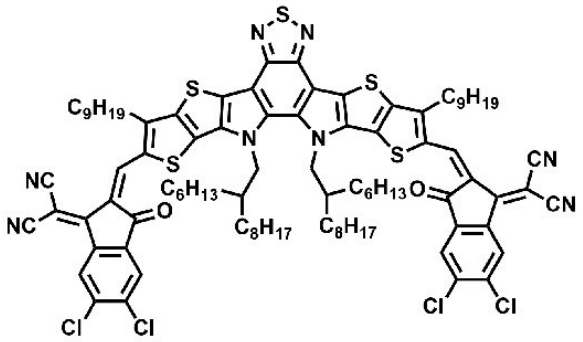

BTP-eC9-HD

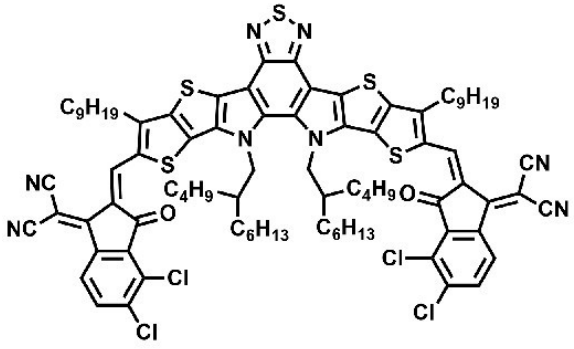

o-BTP-eC9

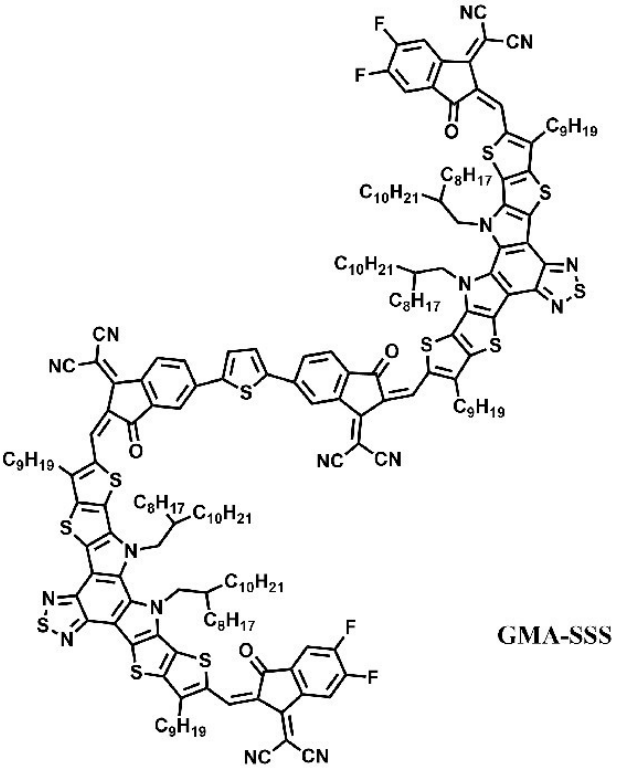

GMA-SSS

Figure S1. Molecular structures of donors and non-fullerene acceptors used in this work.

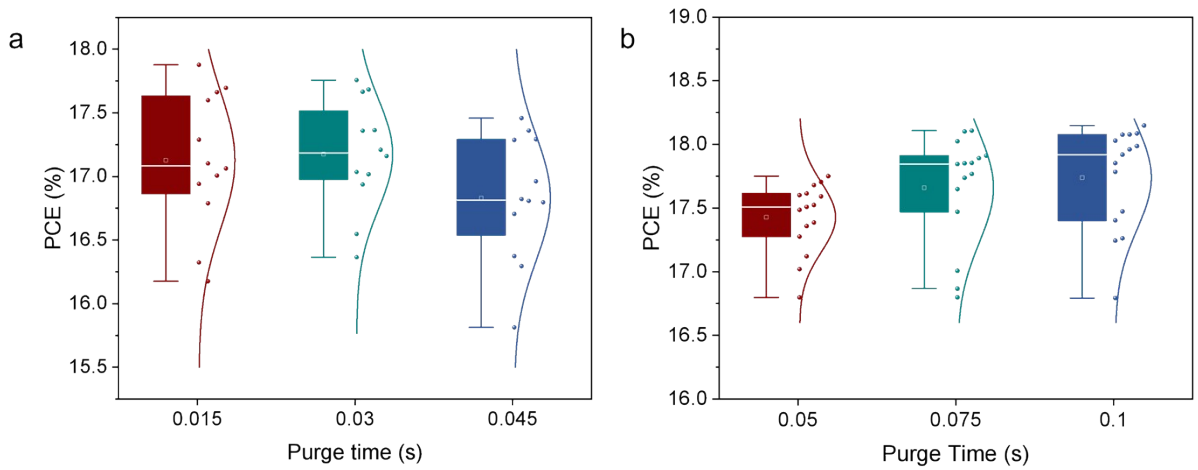

Figure S2. Statistical distribution (box charts) of the PCE for devices fabricated with ALD-SnO_2 ETLs deposited by various purge time of (a) TDMASn, and (b) H_2O.

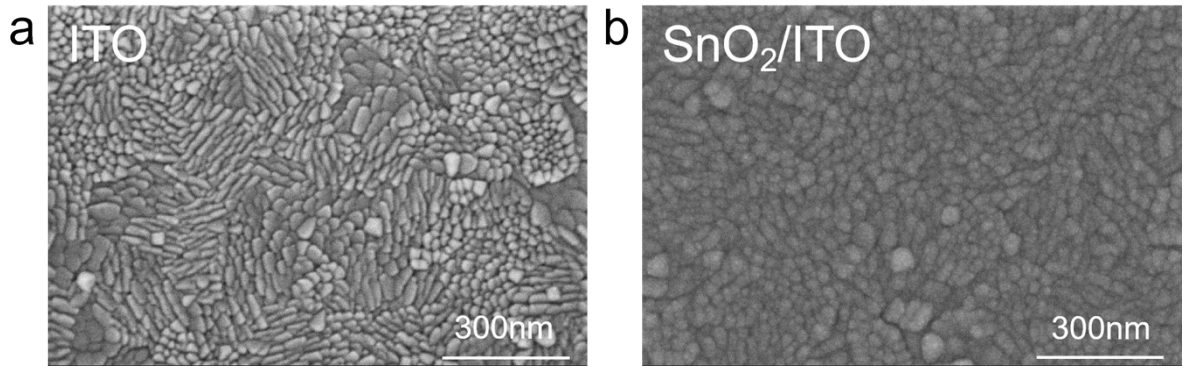

Figure S3. SEM images of (a) ITO films and (b) ALD-SnO2 films deposited on glass/ITO substrates.

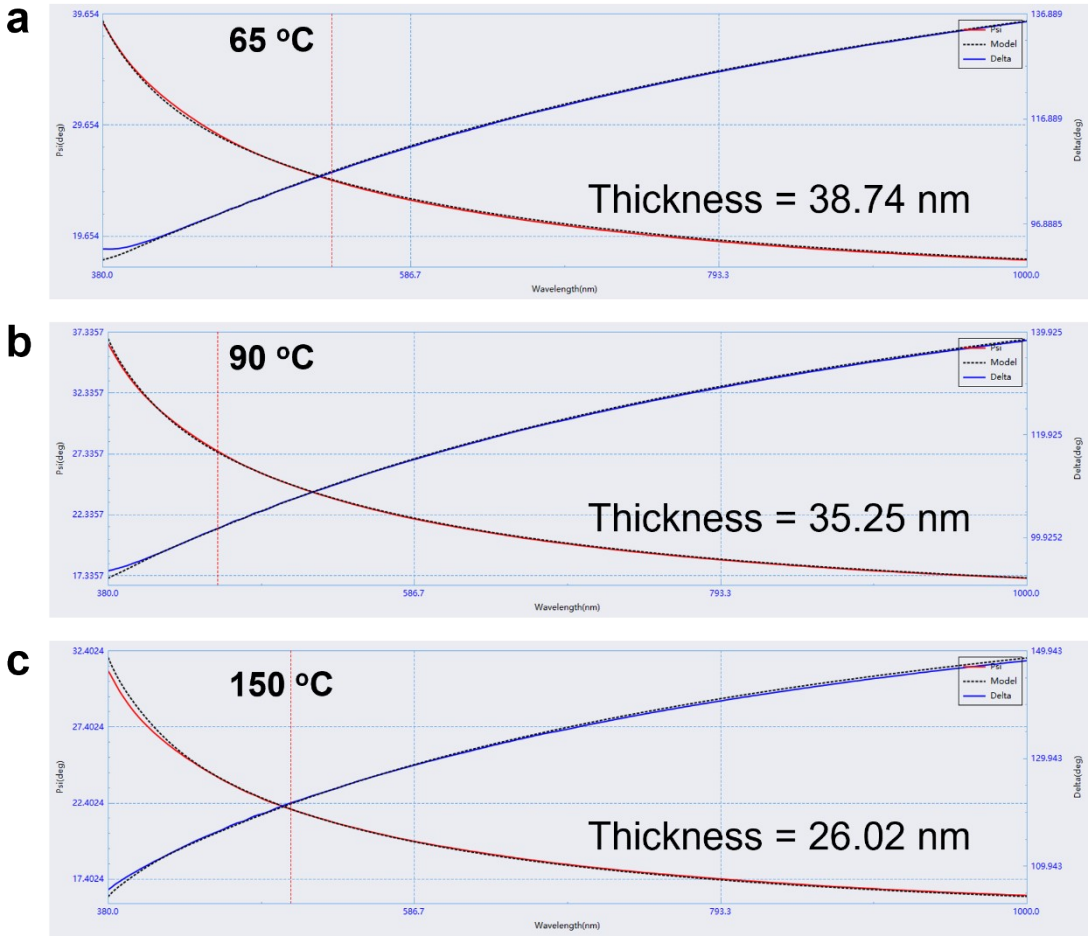

Figure S4. The thickness determination of ALD-SnO_2 using ellipsometry, and thickness per cycle is summarized in below **Table S1**.

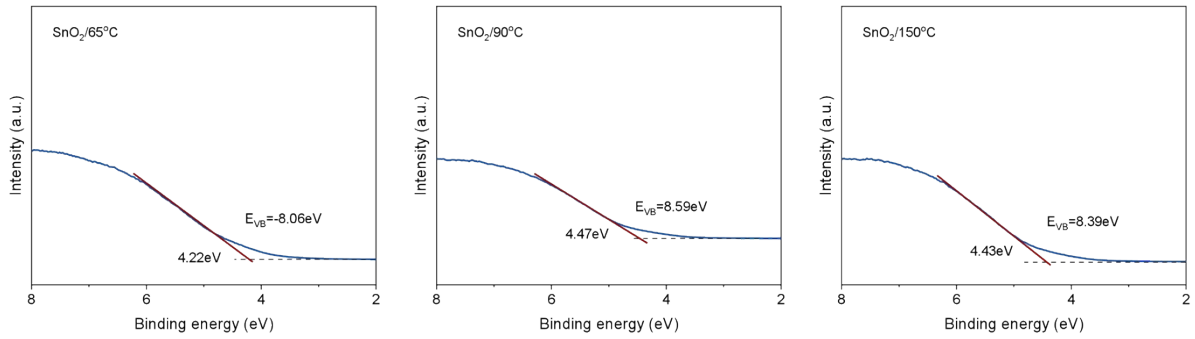

Figure S5. UPS spectra in the valance band region of SnO_2 films deposited at different temperatures.

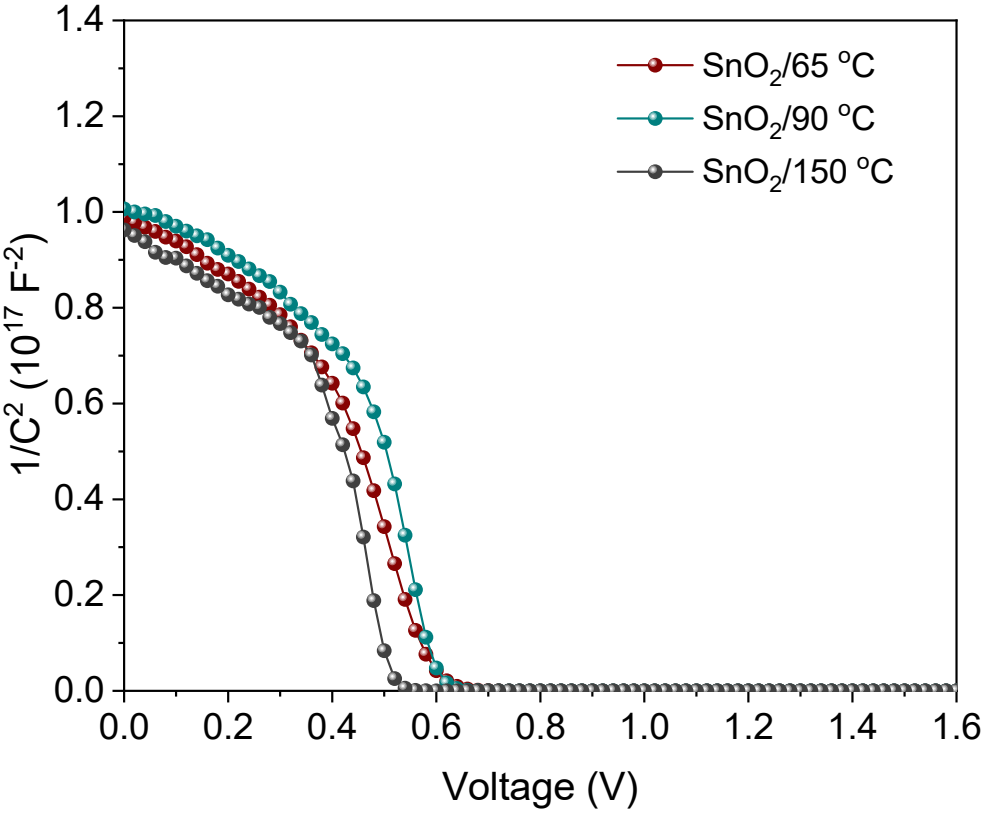

Figure S6. Mott-Schottky plots of OSCs devices fabricated with ALD-SnO_2 films deposited at different temperatures.

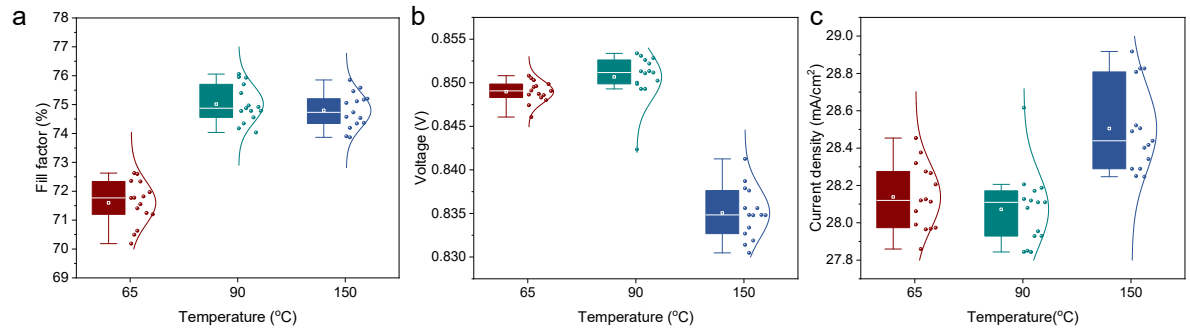

Figure S7. Statistical distribution (box charts) of the Fill factor, Voltage and Current density for devices fabricated with ALD-SnO_2 films deposited at various temperatures.

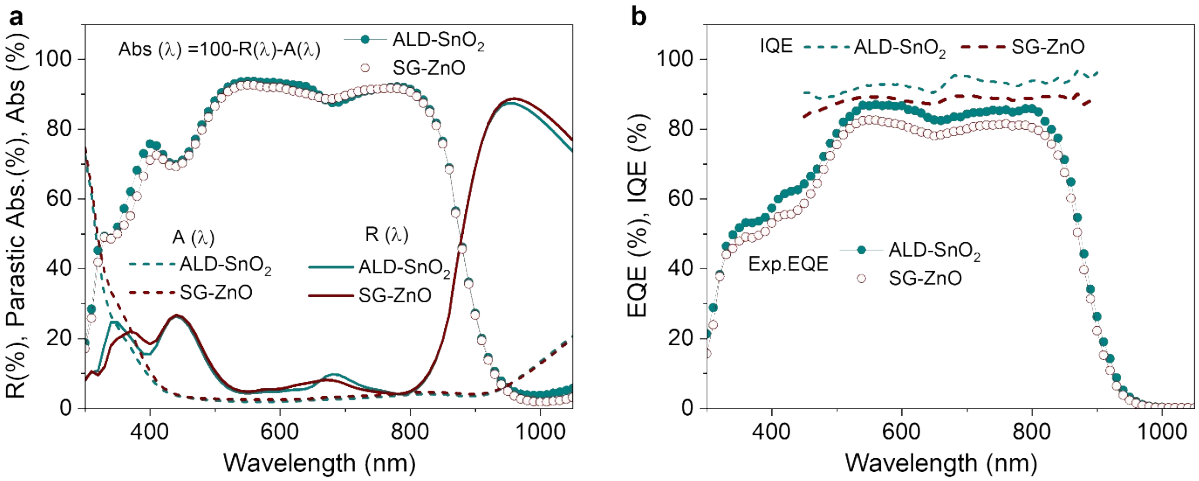

Figure S8. IQE comparison for ALD-SnO_2 and SG-ZnO based PM6:BTP-eC9 (CB) devices. IQE(λ) = Exp. EQE(λ)/100–R(λ)–A(λ), where R(λ) is the measured reflectance of the device and A(λ) is the parasitic absorption of non-active layers in the devices calculated by transfer matrix method. (a) measured R(λ), calculated A(λ) and absorption of active layer in stack (=100–R(λ)–A(λ)). (b) Experimental EQE and calculated IQE.

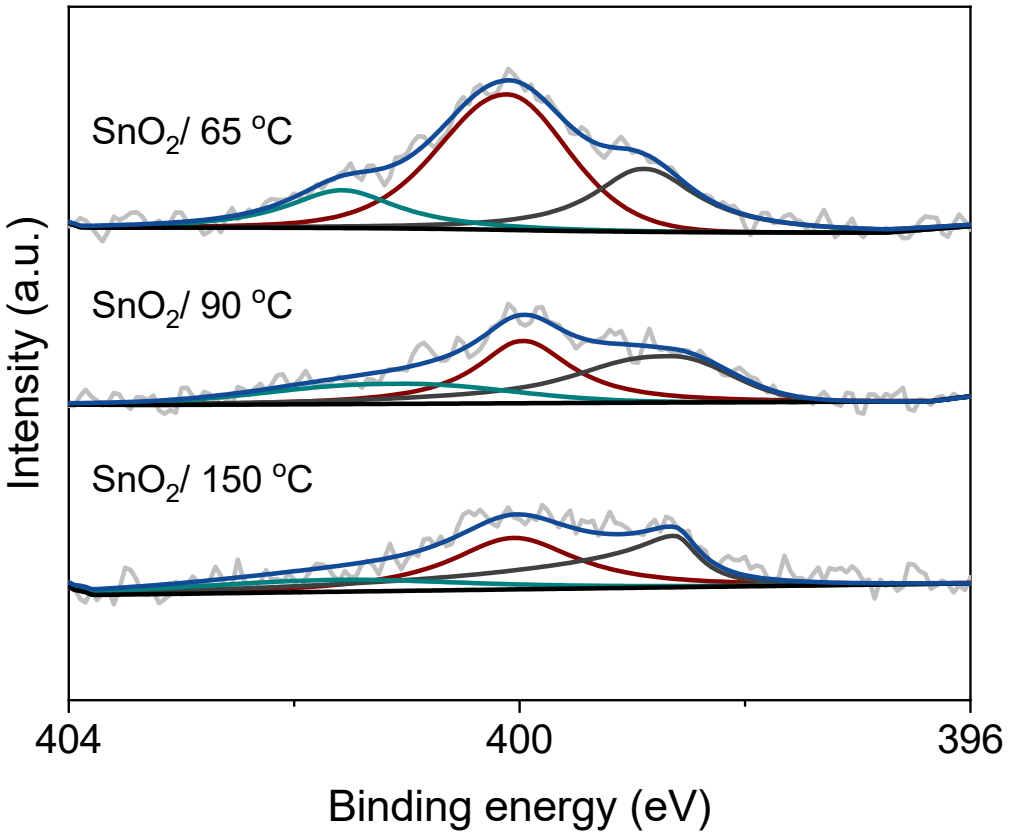

Figure S9. High-resolution XPS spectra of N1s of SnO_2 films deposited at different temperature.

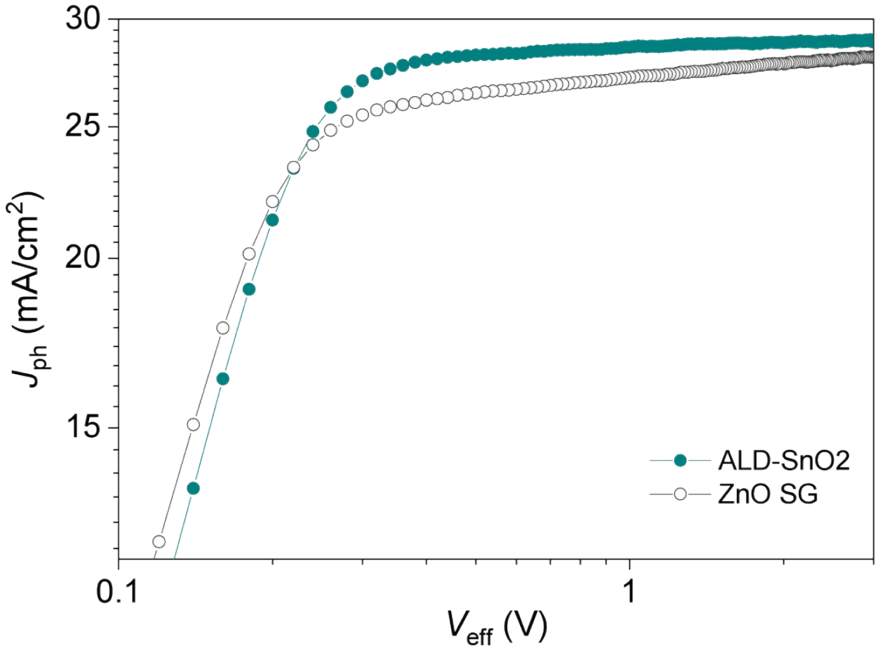

Figure S10. J_{ph}–V_{eff} curves of the OSCs devices fabricated with ALD-SnO_2 and SG-ZnO.

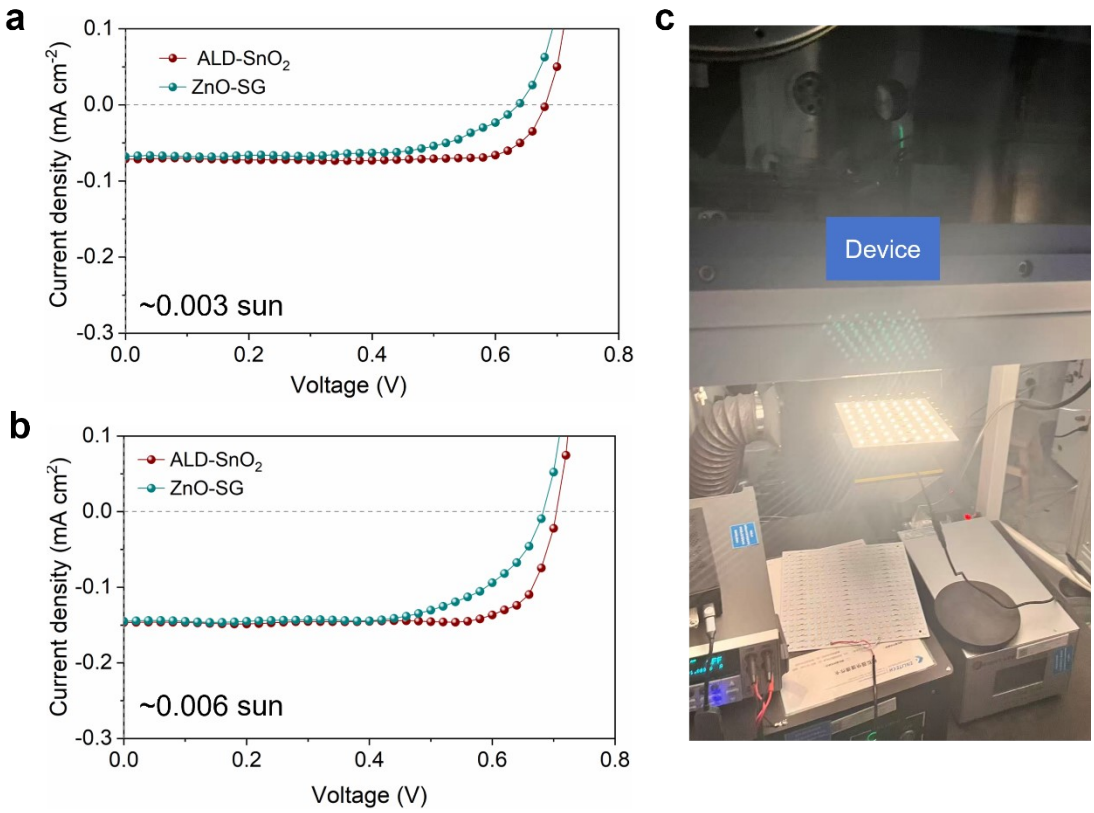

Figure S11. *J-V* characteristics of PM6: BTP-eC9-based organic solar cells employing ALD-SnO_2 and ZnO-SG as electron transport layers. Devices were measured under weak LED illumination at equivalent intensities of (a) ~0.003 sun and (b) ~0.006 sun. (c) Photograph of the LED light source setup used for low-light characterization. All measurements were performed inside a nitrogen-filled glovebox.

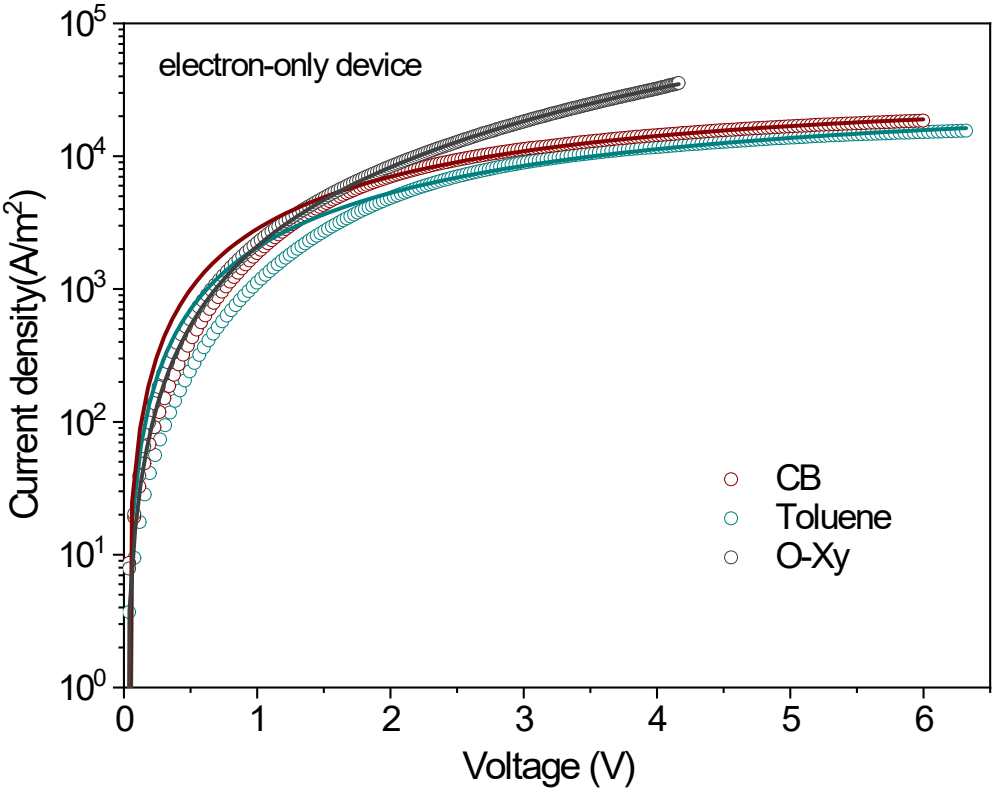

Figure S12. Electron mobility of PM6: BTP-eC9-based OSCs prepared with different solvents.

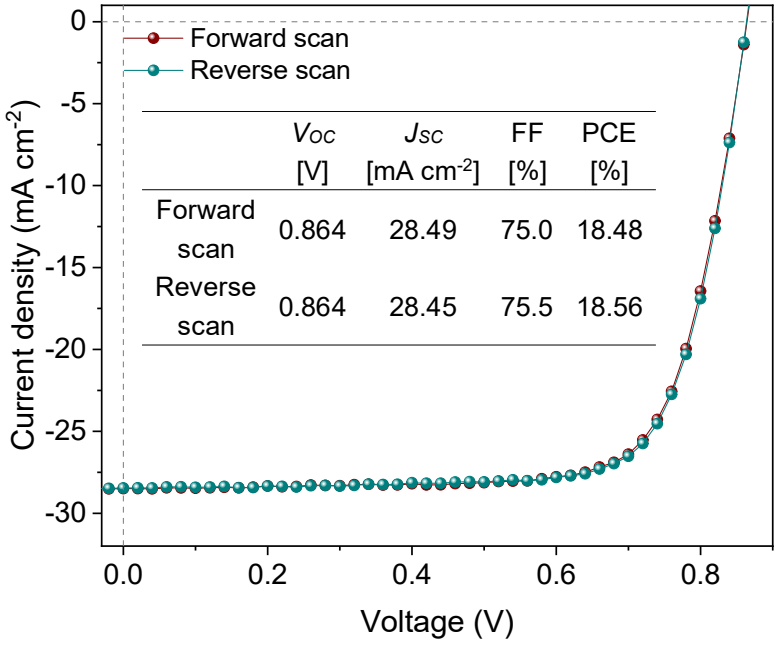

	V_{OC} [V]	J_{SC} [mA cm^{-2}]	FF [%]	PCE [%]
Forward scan	0.864	28.49	75.0	18.48
Reverse scan	0.864	28.45	75.5	18.56

Figure S13. Forward and reverse scan for the optimized ALD-SnO_2 based device.

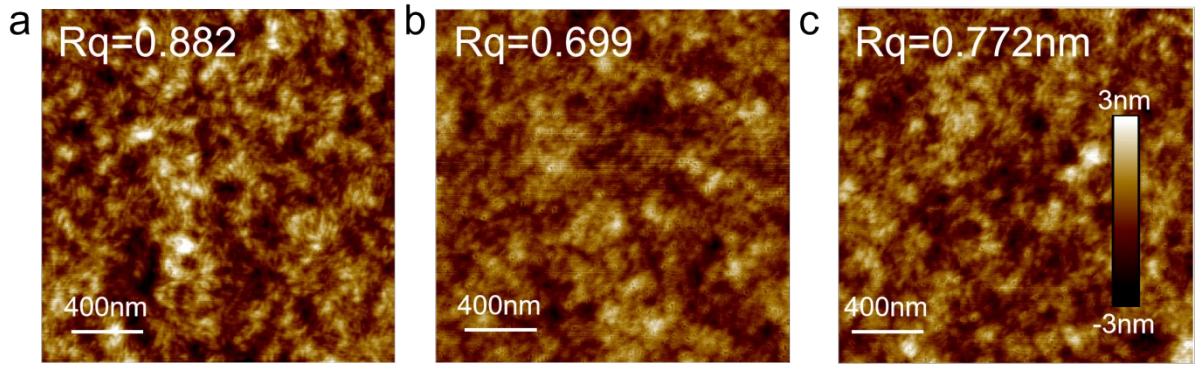

Figure S14. AFM height images of blend films dissolved in (a) CB, (b) Toluene and (c) o-Xy.

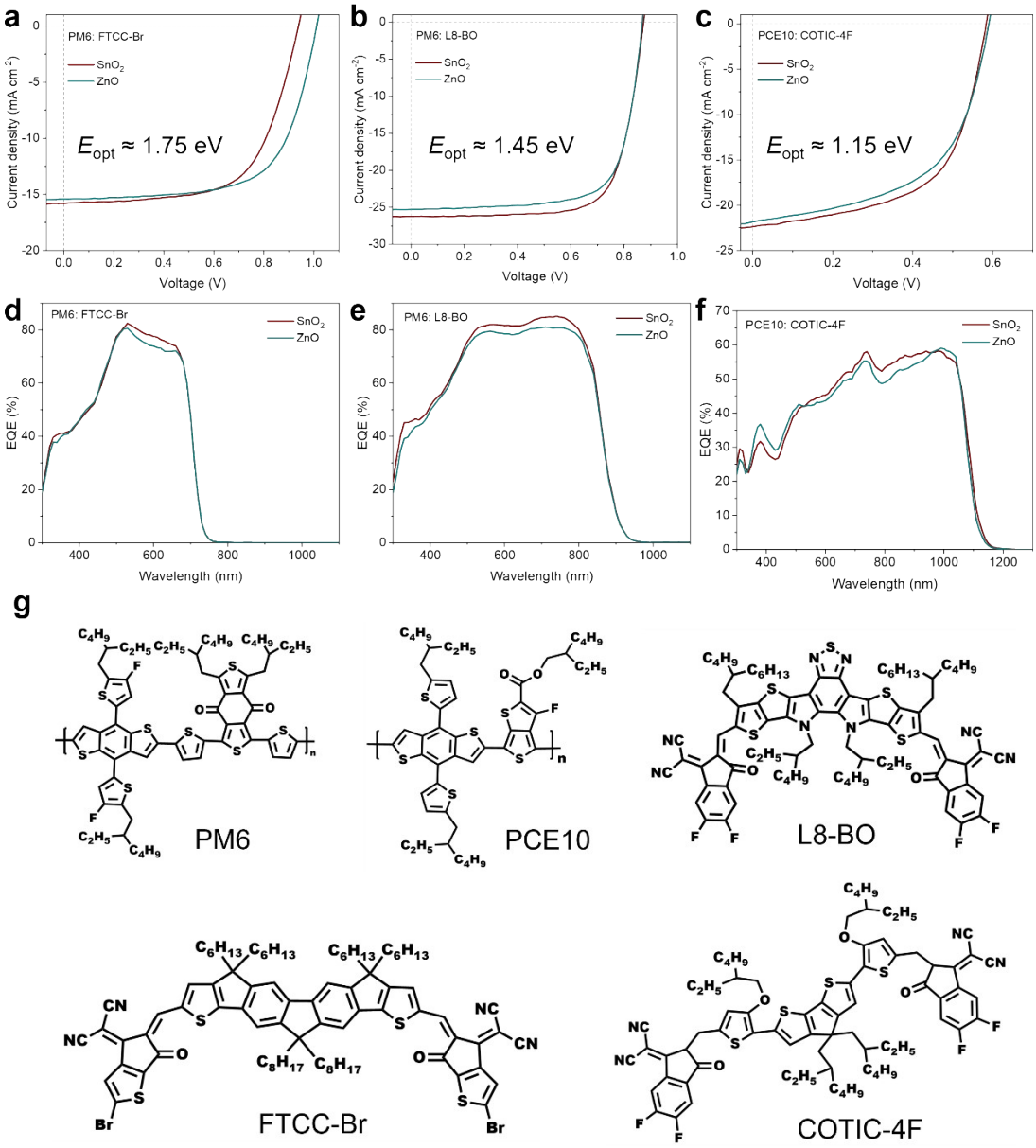

Figure S15. *J-V* characteristics of OSC devices based on (a) PM6: FTCC-Br, (b) PM6:L8-BO, and (c) PCE10: COTIC-4F active layers, comparing ALD-SnO_2 and ZnO ETLs. (d-f) the corresponding EQE curves. (g) the chemical structure of the used materials.

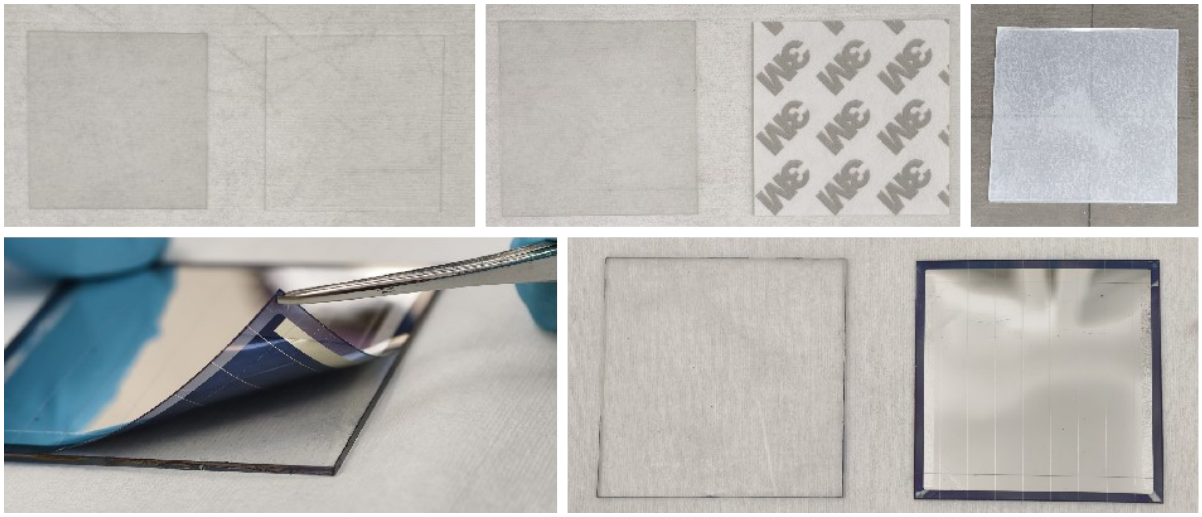

Figure S16. Photograph images of process of attaching PEN flexible substrates to glass and peeling off flexible organic solar modules from glass.

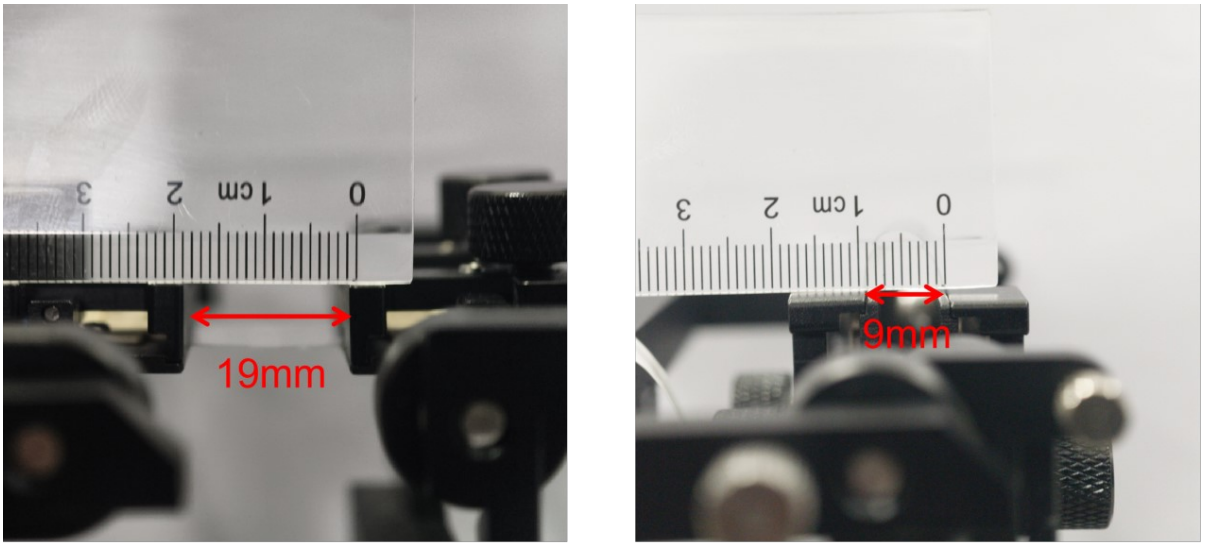

L(Sample clamping distance) = 19 mm
D(The distance between the clamps) = 9 mm
∵R(Bending radius) < L
∴R= D/2 = 4.5 mm

Figure S17. Calculation of the bending test radius for flexible devices.

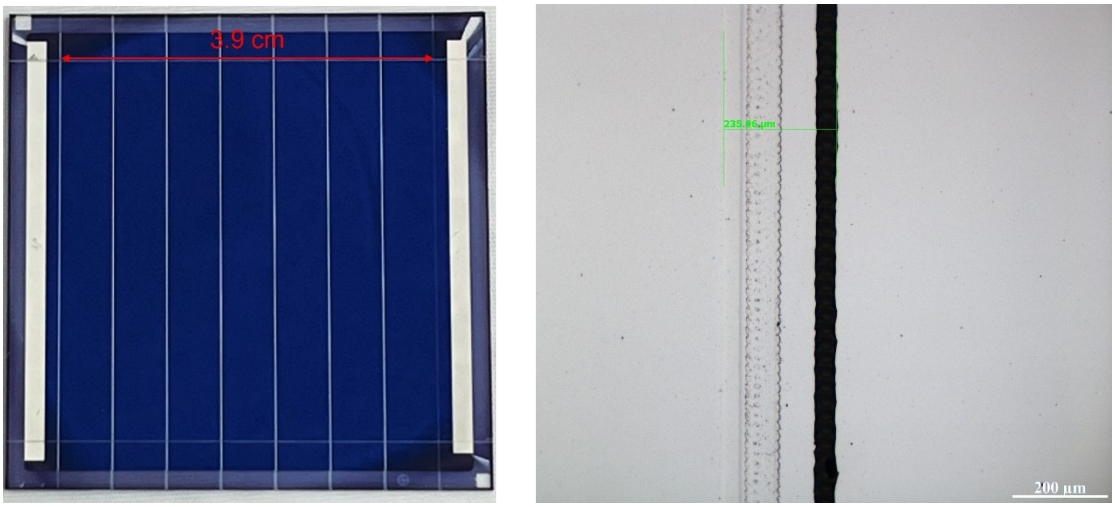

Figure S18. Schematic layout of the series-connected rigid OSC module and the aperture area is 15.6 cm^2. The image of P1-P2-P3 dead zone is shown on the right and the geometric fill factor (GFF) is calculated as GFF = (3.9 cm−6×0.0236 cm) ÷3.9 cm = 96.36%.

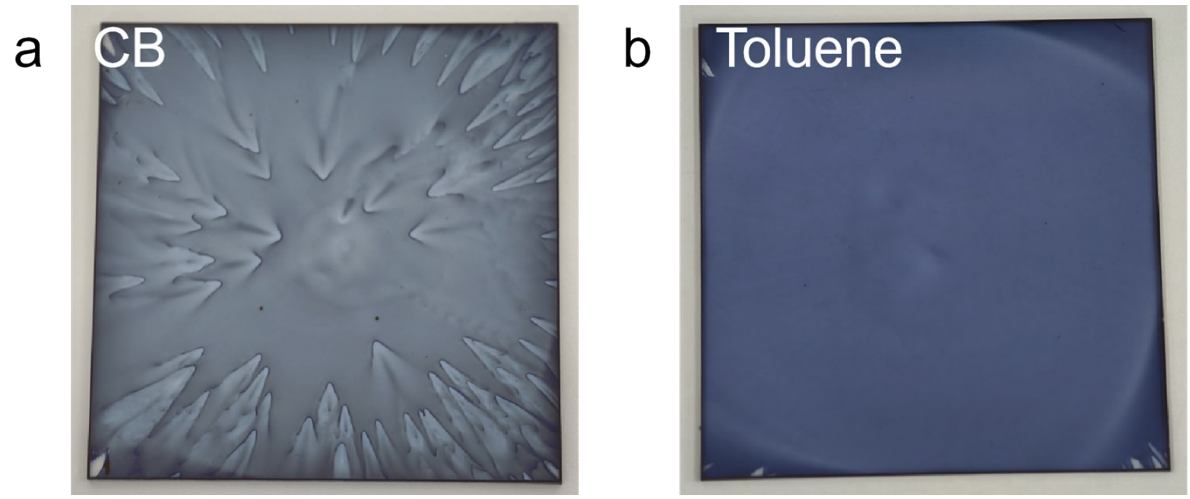

Figure S19. Photograph images of the active layer coated on the 5cm × 5cm substrate using toluene and CB as the solvent.

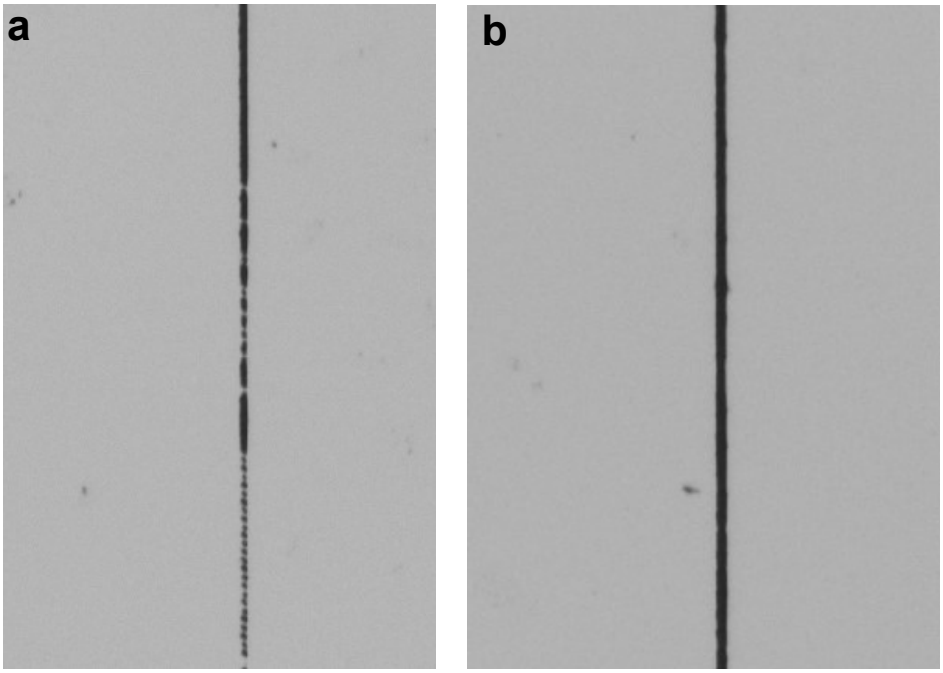

Figure S20. Both partially etched (a) and fully etched (b) Ag layers could often occur on the same module under identical P3 processing parameters.

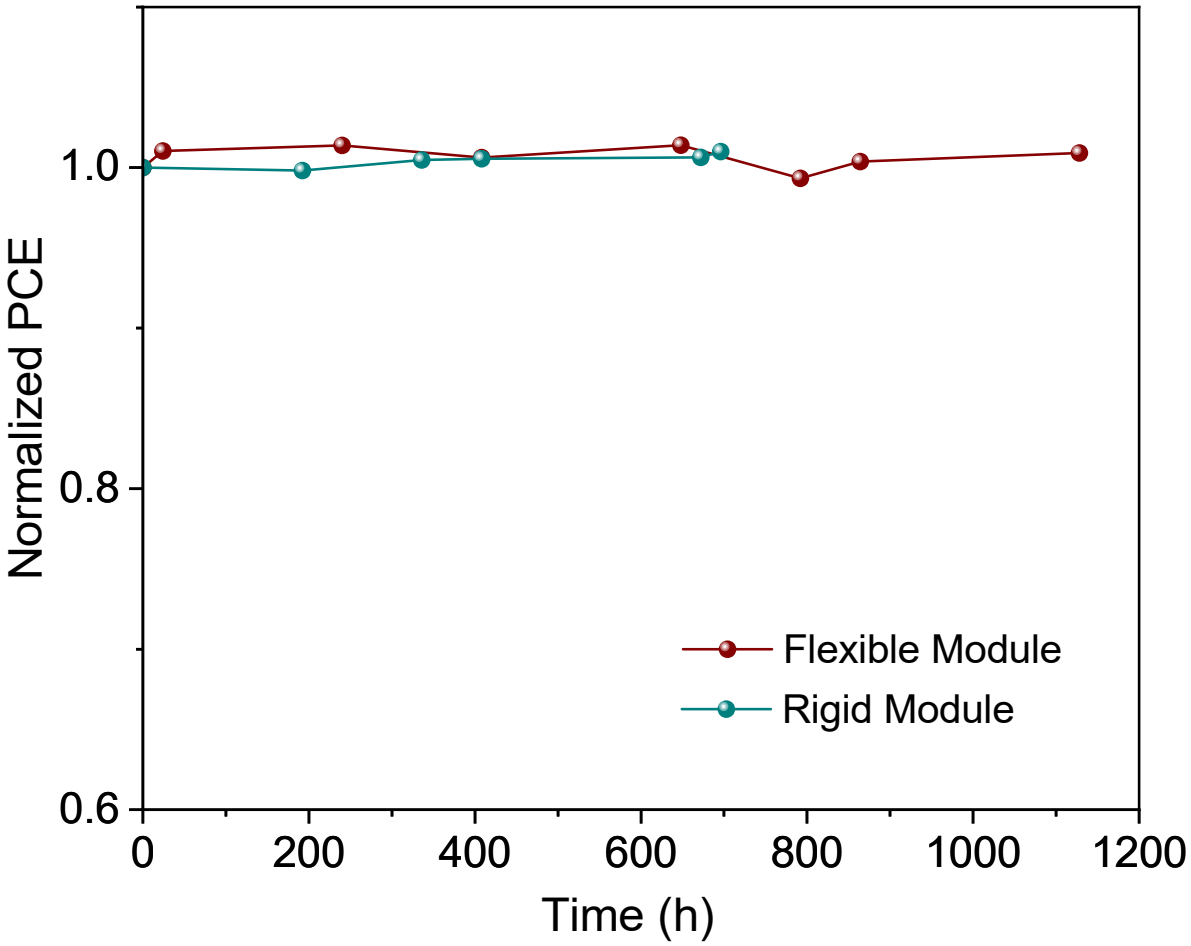

Figure S21. Storage stability of the non-encapsulated organic solar modules.

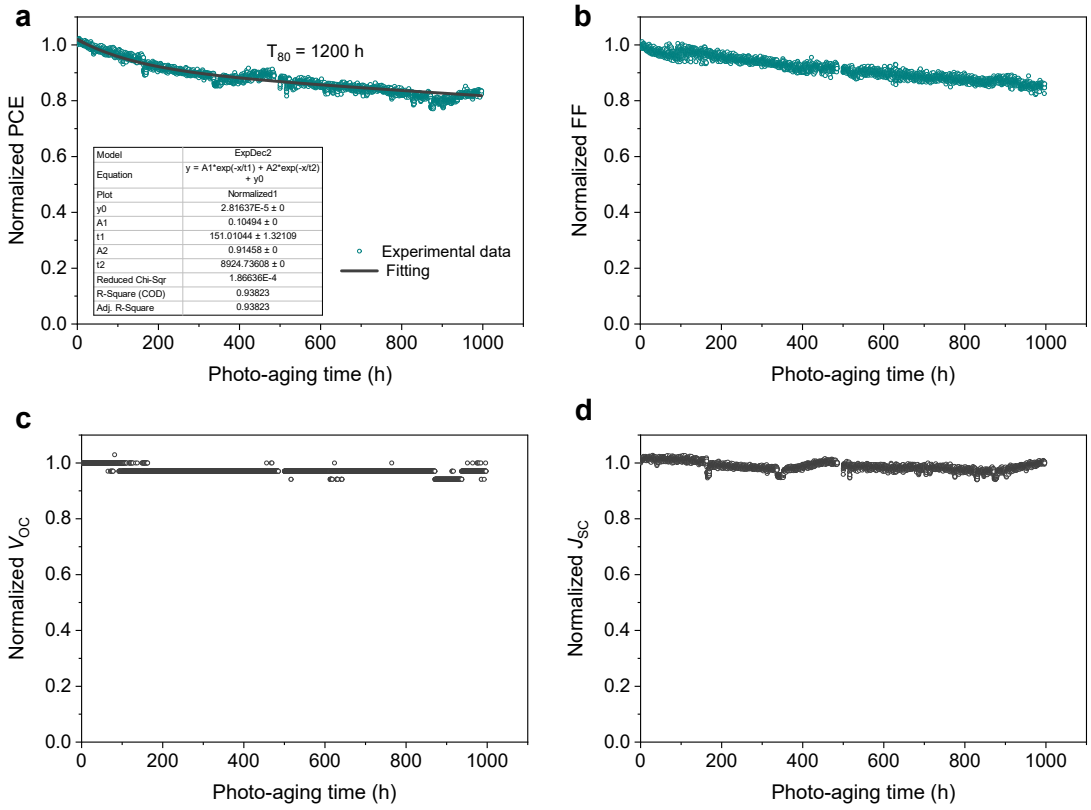

Figure S22. Degradation evolution of photovoltaic parameters under continuous LED illumination (400–1100 nm) at maximum power point tracking (MPPT): (a) PCE, (b) FF, (c) V_{OC}, and (d) J_{SC}.

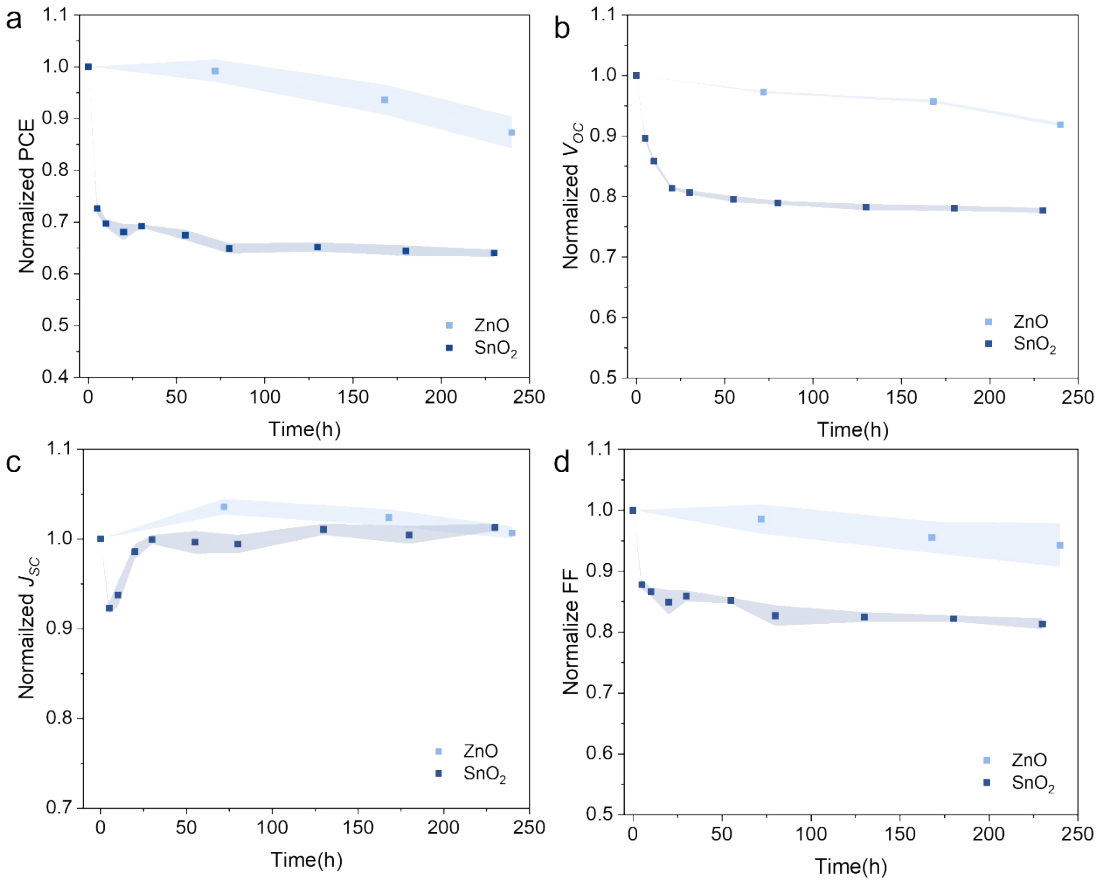

Figure S23. Normalized (a) PCE, (b) V_{OC}, (c)J_{SC}, (d) FF evolutions of the fresh prepared PM6: BTP-eC9 cells under thermal annealing at 85 °C in N_2-filled glovebox. Each data point represents the average value of over four devices.

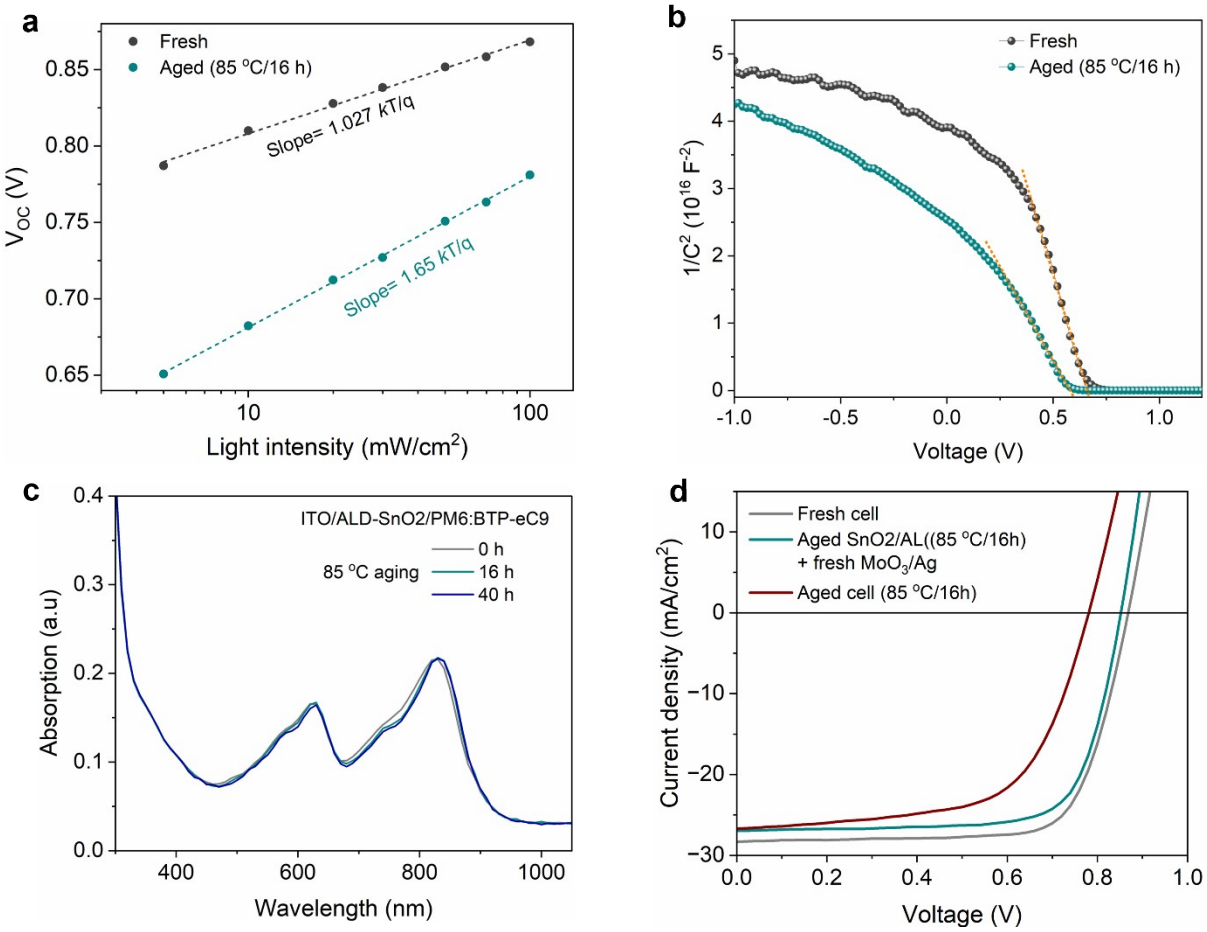

Figure S24. (a) Semi-log plots of measured Voc as a function of light intensity for fresh and aged inverted devices based on ALD-SnO_2 with a PM6: BTP-eC9 blend. The dash lines present the best linear fits and the slopes are indicated. (b) The corresponding Mott–Schottky plots of fresh and aged devices, measured at 2kHz in the dark. (c) Absorption evolution of PM6: BTP-eC9 film on ITO/ALD-SnO2 substrate during thermal aging at 85°C in a N_2-filled glovebox. (d) J-V curves of fresh and aged cells, and a device where only the ITO/SnO2/active layer stack was pre-aged at 85 °C in a N_2-filled glovebox.

Supplementary Note 1. Analysis of thermal instability in ALD-SnO_2-based solar cells.

As shown in Figure S23, the degradation exhibits a rapid burn-in within the first 20 hours and then continues over 200 hours, with a notable decay in both V_{oc} and FF. To understand the underlying cause, we performed the following experiments. We firstly compared the light intensity dependence of Voc for fresh and aged (85 oC/ 16 h). Fresh device showes a slope of ~1.027 kT/q (Figure S24a), indicating a most ideal bimolecular recombination

is dominant. In contrast, the aged device exhibits a significantly increased slopes of >1.65 kT/q, which is characteristic of trap-assisted Shockley–Read–Hall (SRH) recombination. This suggests that thermal aging introduces additional trap states into the active layer. To further verify the increased trap density, we performed Mott–Schottky measurements (Figure. 24b). The aged devices display a markedly reduced slope in the $(C/A)^{-2}$ vs. V plot, approaching a straight line (slope ~ $1/N_t$). According to the relation:

$$N_t = -\frac{2}{q\varepsilon_0\varepsilon_r}\left(\frac{d(C/A)^{-2}}{dV}\right)^{-1}$$

where ε_0 is the dielectric constant of the vacuum, ε_r is the relative dielectric permittivity of the doped active material ($\varepsilon_r = 3.5$), and A is the device area. This behavior indicates a significant increase in the unintentional n-doping density within the non-fullerene acceptor (NFA) blend film. The reduced slope is consistent with a higher concentration of ionized dopants or traps.

To examine whether the SnO_2 interface chemically reacts with the blend, we fabricated a thinner active layer (total blend concentration 6.6 mg/mL) and tracked absorption under continuous aging. After 16 hours, we observe only a slight red-shift at the absorption edge, which remains stable with prolonged aging. This minor change does not strongly support a chemical reaction between SnO_2 and the blend; rather, it is more consistent with thermally induced morphological aggregation (increased crystallization in NFA). This interpretation is further supported by Figure S24d, where the device with pre-aged ITO/SnO_2/blend (without top electrode) shows only a modest V_{oc} reduction. Thus, the fast degradation cannot be fully attributed solely to the ALD-SnO_2/blend interface.

We note a recent study by Ma et al. (*ACS Appl. Mater. Interfaces* 2025, 17, 15456–15467), which reports that under thermal aging, MoO_3 at the top interface can partially reduce from Mo^{6+} to Mo^{5+} (forming $(MoO_3)^-$ species),

leading to p-doping of the underlying bulk heterojunction (BHJ) layer. If a similar top-doping mechanism were dominant in our devices, we would expect comparable degradation in ZnO-based control devices. However, the ZnO-devices remain substantially more stable under the same 85 °C aging conditions. This observation suggests that the degradation mechanism is more complex and likely involves multiple interfaces. At this stage, we cannot definitively conclude that detrimental interfacial reactions are the primary cause of degradation, given that the absorption changes are minor. Nevertheless, the combined evidence of increased SRH recombination, higher apparent doping density from Mott–Schottky, and the selective instability of SnO_2 based devices, points toward unintentional doping as a key factor. One plausible origin is residual impurities from the ALD precursor (tetrakis dimethyl amino tin, TDMASn). If the Sn–N bonds are not fully cleaved and oxidized to SnO_2, residual TDMASn or related species may remain as mobile impurities that diffuse into the blend and act as dopants. This effect can be exacerbated in a complete device, rather than in a doped film alone.

Table S1. The summary of ALD-SnO2 deposited at different substrate temperature.

ALD-deposition cycle	ALD-deposition temperature	Thickness	Thickness/cycle
252	65 ℃	38.74 nm	1.54 Å
	90 ℃	35.25 nm	1.40 Å
	150 ℃	26.02 nm	1.03 Å

Note: The value of goodness of fit (GOF) for each sample is closed to unit.

Table S2. Photovoltaic parameters for inverted PM6:BTP-eC9 (1:1.2,wt/wt) solar cells fabricated with ALD-SnO2 films deposited at different temperatures under AM 1.5G solar illumination at 1000 W m^{-2}.

Temperature [℃]	J_{SC} [mA cm^{-2}]	V_{OC} [V]	FF [%]	PCE[a] [%]
65	28.14 ± 0.22	0.849 ± 0.001	71.5 ± 0.6	17.09 ± 0.19 (17.42)
90	28.13 ± 0.24	0.851 ± 0.001	75.2 ± 0.7	18.00 ± 0.16 (18.18)
150	28.57 ± 0.25	0.833 ± 0.002	74.8 ± 0.7	17.80 ± 0.19 (18.16)

The average values and standard deviations are obtained from over 15 devices, and all the devices use the same fabrication parameters.

Table S3. Photovoltaic parameters for inverted PM6:BTP-eC9 (1:1.2,wt/wt) solar cells fabricated with ALD-SnO2 films of different thicknesses under AM 1.5G solar illumination at 1000 W m^{-2}.

Thickness [nm]	J_{SC} [mA cm^{-2}]	V_{OC} [V]	FF [%]	PCE[a] [%]
2	28.90 ± 0.32	0.764 ± 0.008	64.6 ± 0.6	14.27 ± 0.38 (14.81)
10	28.13 ± 0.24	0.851 ± 0.001	75.2 ± 0.7	18.00 ± 0.16 (18.18)
25	28.92 ± 0.17	0.840 ± 0.002	73.5 ± 0.7	17.87 ± 0.12 (17.97)

The average values and standard deviations are obtained from over 15 devices, and all the devices use the same fabrication parameters.

Table S4. Detailed PV parameters for PM6: BTP-eC9 based devices using ZnO SG and ALD-SnO_2 ETLs, measured under weak LED illumination.

ETL	J_{SC} [μA cm^{-2}]	V_{OC} [V]	*FF* [%]	Light intensity
ZnO SG	68 ± 1	0.637 ± 0.002	64.7 ± 2.6	0.003 sun
ALD-SnO_2	72 ± 1	0.681 ± 0.003	79.4 ± 1.4	
ZnO SG	145 ± 2	0.681 ± 0.006	66.8 ± 1.4	0.006 sun
ALD-SnO_2	148 ± 2	0.704 ± 0.003	79.8 ± 1.2	

Note: The light intensity was calibrated using a reference silicon cell, with the equivalent sun intensity determined by comparing the current density generated under LED illumination to that measured under standard AM 1.5G illumination.

Table S5. Photovoltaic parameters for inverted PM6:BTP-eC9 (1:1.2,wt/wt) solar cells fabricated with ALD-SnO2 films of different thicknesses under AM 1.5G solar illumination at 1000 W m^{-2}.

Solvent	J_{SC} [mA cm^{-2}]	V_{OC} [V]	FF [%]	PCE[a] [%]
O-Xylene	28.01 ± 0.09	0.816 ± 0.003	68.6 ± 0.2	15.70 ± 0.13 (15.88)
Toluene	28.13 ± 0.24	0.851 ± 0.001	75.2 ± 0.7	18.00 ± 0.16 (18.18)
CB	27.73 ± 0.23	0.865 ± 0.002	75.9 ± 0.4	18.21 ± 0.18 (18.45)

The average values and standard deviations are obtained from over 15 devices, and all the devices use the same fabrication parameters.

Table S6. Mobility results of the SCLC devices based on PM6：BTP-eC9 blends in different solvents.

Solvent	μh [cm2 V^{-1} s^{-1}]	μe [cm^2 V^{-1} s^{-1}]
CB	2.67E-03	1.22E-04
Toluene	4.04E-03	3.67E-04
O-Xy	9.71E-04	1.08E-04

Device area is 0.09cm^2 and was measured under dark conditions without the use of a mask.

Table S7. GIWAXS characteristics of the blend films.

Crystallographic parameters			CB	Toluene	O-Xy
IP[a]	Lamellar packing (100)	q (Å−1)	0.315	0.311	0.299
		d-spacing (Å)	19.937	20.193	21.003
OOP[b]	π–π Stack (010)	q (Å−1)	1.683	1.671	1.626
		d-spacing (Å)	3.731	3.758	3.862
		FWHM ($Å^{-1}$)	0.410	0.391	0.401
		Coherence Length (Å)	13.785	14.455	14.095

[a]IP and [b]OOP indicate in-plane and out-of-plane, respectively.

Table S8. Photovoltaic parameters of the best ternary OSCs device with different third components (PM6:BTP-eC9:NFA = 1:1:0.2) under AM 1.5G solar illumination at 1000 Wm^{-2}.All the devices were processed from CB solvent doped with TCB, and SnO_2 as the ETL.

The third component	J_{SC} [mA cm^{-2}]	V_{OC} [V]	FF [%]	PCE[a] [%]
GMA-SSS	28.04	0.872	75.1	18.36
BTP-eC9-HD	28.11	0.863	75.9	18.40
o-BTP-ec9	28.12	0.871	76.1	18.64

Table S9. Detailed photovoltaic parameters for OSCs based on PM6: FTCC-Br (wide gap), PM6:L8-BO (medium gap), and PCE10: COTIC-4F (low gap) with ZnO-SG and ALD-SnO_2 ETLs, measured under 1.5G 1-Sun illumination.

Active Layer	ETL	J_{SC} (J_{EQE}) [mA cm^{-2}]	V_{OC} [V]	*FF* [%]	*PCE*[a] [%]
PM6: FTCC-Br	ZnO SG	15.42 ± 0.18 (14.47)	1.016 ± 0.004	64.9 ± 1.1	10.13 ± 0.22 (10.39)
	ALD-SnO_2	15.56 ± 0.23 (14.77)	0.935 ± 0.004	63.4 ± 0.6	9.20 ± 0.20 (9.45)
PM6:L8-BO	ZnO SG	24.81 ± 0.47 (23.57)	0.866 ± 0.003	73.2 ± 0.4	15.68 ± 0.35 (16.14)
	ALD-SnO_2	25.52 ± 0.37 (24.44)	0.871 ± 0.001	72.7 ± 0.5	16.32 ± 0.29 (16.67)
PCE10: COTIC-4F	ZnO SG	21.87 ±0.40 (20.52)	0.592 ± 0.004	54.9 ± 0.5	7.09 ± 0.12 (7.24)
	ALD-SnO_2	22.05 ± 0.30 (21.05)	0.584 ± 0.001	58.7 ± 0.7	7.54 ± 0.16 (7.74)

a) The average values and standard deviations are obtained from over 15 devices, and all the devices use the same fabrication parameters. Note that the active layer solutions were prepared as follows: PM6: FTCC-Br (1:1 wt/wt) with PM6 concentration of 10 mg/mL in CB; PM6:L8-BO (1:1.2 wt/wt) with PM6 concentration of 10 mg/mL in chlorobenzene (CB); and PCE10: COTIC-4F (1:1.5 wt/wt) with PCE10 concentration of 8 mg/mL in CB. All the blend solution was stirred and spin-coated at 85°C, with 10 mg/mL TCB added as additive.

Table S10. Comparison with literature reported **flexible organic solar cells**.

Active Materials	V_{OC} [V]	J_{SC} [mA/cm^2]	FF [%]	PCE [%]	Device structure/solvent	Ref.
D18:Y6:Y6-1O	0.908	26.78	80.17	19.51	Direct/CF	1
PM6:BTP-eC9:L8-BO:1000k-PEO	0.878	27.64	78.75	19.12	Direct/O-Xy	2
PM6:L8-BO	0.86	26.2	73.1	16.47	Inverted/CF	3
PM6:Y6	0.85	26.91	73.77	16.87	Direct/CF	4
PM6:BTP-BO-4Cl:C-PC61BM	0.813	26.75	75.08	16.33	Inverted/CF	5
PM6:L8-BO:ZY-4Cl	0.905	26.11	78.31	18.51	Direct/CF	6
D18:L8-BO:F-GS-ISO	0.926	26.19	76.68	18.6	Direct/CF	7
D18:L8-BO	0.89	25.46	73.26	16.52	Direct/CF	8
PM6:D18:BTP-eC9	0.847	27.68	80.35	18.84	Direct/CF	9
D18:L8-BO	0.92	26.1	76.5	18.3	Direct/CB	10
D18:Y6:PC71BM	0.854	27.15	77.49	18	Inverted/CF	11
D18/PM6-b-PYSe/BTP-eC9	0.87	27.46	75.2	17.97	Direct/CB	12
D18:Y6:PC71BM	0.86	26.94	76.48	17.72	Inverted/CF	13
PM6:L8-BO	0.879	25.25	76.81	17.07	Inverted/CF	14
D18:N3:DOY-C4	0.853	27.34	76.8	17.91	Direct/CF	15
PM6:BTP-eC9	**0.861**	**27.6**	**75.8**	**18.03**	**Inverted/CB**	**This work**

Table S11. Overview of recently published **rigid organic solar** mini-modules to date.

Active Materials	Active Area [cm^2]	Active PCE [%]	Device structure	Ref.
PM6: BO-4Cl	13.5	15.02	Inverted	16
PM6: BTP-eC9: QD-1	13.5	17.33	Direct	17
PM6: BTP-eC9	16.94	15.87	Inverted	18
PM6: L8BO: PC61BM	11.08	16.1	Inverted	19
PM6: BDTF-CA2O: BTP-eC9	14.82	17.68	Direct	20
D18: PM6: N3: L8-BO	20.33	16.27	Inverted	21
PM6: D18: L8-BO	15.64	16.03	Direct	22
PM6: BTP-eC9	14.9	17.28	Direct	23
PM6: D18: BTP-eC9	15.6	16.7	Direct	24
D18: BO-4Cl: L8-BO	16.94	17.05	Direct	25
D18: L8-BO	19.3	15.44	Direct	26
PM6: BO-4Cl	18.92	16.07	Direct	27
PM6: BTP-BO-4Cl	18.73	14.79	Direct	28
PM6: PC71BM: BTP-ec9	12.2	13.07	Direct	29
PM6: DTY6	18	14.4	Direct	30
PM6: Y6: BTO: PC61BM	36	14.26	Direct	31
PM6:BTP-eC9	25.21	14.07	Inverted	32
PM6: L8-BO	18.73	15.2	Direct	33
PM6: PBQx-TCl: PY-IT	18.72	16.26	Direct	34
PM6: T8	7.5	15.38	Direct	35
PBDB-TFCl: D18-Cl: PY-IT	36.2	15.1	Direct	36
PBQx-TF: eC9-2Cl	21	16.1	Direct	37
D18-Cl: BTP-4F-P2EH	17.6	17	Direct	38
PBQx-TCl: eC9-2Cl	22.17	16.5	Direct	39

PM6:L8-BO:T5	18.03	16.23	Direct	40
PM6:Y6-C12:PC61BM	196.97	15.08	Direct	41
PM6:L8-BO	11.72	16.02	Direct	42
PM6:L8-BO(HU-DT):PC70BM	198.82	11.44	Direct	43
PM6: BTO-BO: L8-BO	15.6	16.35	Direct	44
PM6:BTP-eC9	**15.02**	**17.6**	**Inverted**	**This work**

Table S12. Overview of recently published **flexible organic solar** mini-modules to date.

Active Materials	Active Area [cm2]	Active PCE [%]	Device structure	Ref.
PBDB-T-2F:Y6:PC61BM	39.96	13.2	Inverted	45
PM6:Y7-12	12.15	11.51	Inverted	46
PM6:Qx− 1	30	12.2	Inverted	47
PM6:L8-BO:PJ1	30	13.08	Inverted	48
PM6:BTP-eC9:PC71BM	32.5	12.9	Inverted	49
PM6:BTP-BO-4Cl	52	13.26	Inverted	50
PM6:BTP-eC9:PC71BM	41	13.6	Inverted	51
PM6:BTP-eC9:PC71BM	52	12.66	Inverted	52
PM6:BTP-eC9:PC72BM	11.57	14.21	Inverted	53
PM6:BTP-eC9:PC71BM	52.3	14.78	Inverted	54
PM6:BTP-eC9:PC72BM	64.19	14.07	Inverted	55
PM6:BTP-eC9	32.5	14.3	Inverted	56
PM6:PBQx-TF:PY-IT	25	15.48	Direct	57
PM6:BTP-eC9	**15.02**	**15.2**	**Inverted**	**This work**

Reference

1 J.-D. Chen, H. Ren, F.-M. Xie, J.-L. Zhang, H.-Z. Li, A. S. Ibupoto, Y.-F. Zhang, Y.-Q. Li and J.-X. Tang, *Nat. Commun.*, 2025, **16**, 3829.

2 R. Gong, Q. Yan, Z. Xing, H. Wang, L. Tan, X. Meng, X. Hu and Y. Chen, *Adv. Mater.*, 2025, **37**, 2501033.

3 M. Yu, H. Shi, L. Hu, M. Du, S. Lan, Y. Jin, J. Yao, M. Du, Z. Yan, E. Zhou and Z. Li, *Surf. Interfaces*, 2025, **65**, 106538.

4 E. Cho, S. Park, S. Cho and S.-J. Lee, *Appl. Surf. Sci.*, 2026, **717**, 164789.

5 Y. Chen, C. Yue, W. Xiong, Y. Han, H. Xu, K. Shui, S. Yang, J. Qin, L. Zhang, Z. Li, Y. Zhang, W. Li, C. Ma and Q. Luo, *Adv. Mater.*, 2025, e10780.

6 R. Ding, S. Wang, Z. Yang, J. Weng, C. Li, Z. Liu, Z. Zhang, J. Zhang, Z. Tang, Y. Cai and H. Huang, *J. Mater. Chem. A*, 2025, **13**, 33356–33364.

7 J. Gao, S. Wang, C. Li, Z. Han, J. Lv, N. Yu, J. Wang, L. Wang, X. Meng, J. Zhang, Z. Tang, Y. Cai and H. Huang, *Adv. Funct. Mater.*, 2025, e21502.

8 Y. Tong, H. Liu, W. Xiao, G. Jiang, S. Gong, Z. Wang, S. Yan and B. Xu, *Adv. Mater.*, 2025, **37**, e09995.

9 J. Xia, J. Zhu, H. Chen, G. Zeng, J. Wan, B. Zhang, S. Lee, J. Xu, J. Cao, X. Wu, J. Ding, L. Yang, W. Chen, C. Yang, Y. Li and Y. Li, *Angew. Chem., Int. Ed.*, 2025, **64**, e202501270.

10 X. Liu, S. Lee, H. Chen, Y. Lin, J. Yu, W. Liu, H. Xu, W. Zhu, C. Yang and X. Song, *Adv. Funct. Mater.*, 2025, e15595.

11 H. Ren, W.-S. Chen, J.-D. Chen, J.-P. Yang, Y.-F. Zhang, H.-Y. Hou, S. Tian, H.-R. Ge, Y.-Q. Li and J.-X. Tang, *Chem. Eng. J.*, 2024, **481**, 148498.

12 D. Zhang, Y. Wu, C. Yan, P. Cheng, G. Zhang, H. Yang and C. Cui, *Adv. Funct. Mater.*, 2024, **34**, 2407681.

13 Y. Zhang, H. Ren, J. Chen, H. Hou, H. Liu, S. Tian, W. Chen, H. Ge, Y. Li, H. Mao, Z. Su and J. Tang, *Adv. Funct. Mater.*, 2023, **33**, 2212260.

14 Z. Wang, J. Guo, Y. Pan, J. Fang, C. Gong, L. Mo, Q. Luo, J. Lin and C. Ma, *Energy Environ. Mater.*, 2024, **7**, e12592.

15 Q. Ye, Z. Chen, D. Yang, W. Song, J. Zhu, S. Yang, J. Ge, F. Chen and Z. Ge, *Adv. Mater.*, 2023, **35**, 2305562.

16 Z. Suo, L. Li, J. Liu, Z. Yao, C. Li, X. Wan and Y. Chen, *Adv. Funct. Mater.*, 2024, **34**, 2409699.

17 W. Shi, Q. Han, W. Zhao, R. Wang, L. Li, G. Song, X. Chen, G. Long, Z. Yao, Y. Lu, C. Li, X. Wan and Y. Chen, *Energy Environ. Sci.*, 2025, **18**, 5356–5364.

18 Y. Cui, H. Li, S. Zeng, K. Zhang, H. Wang, S. Liu, L. Ye, R. Guo, X. Hu and Y. Chen, *Adv. Funct. Mater.*, 2025, **35**, 2414317.

19 E. Feng, C. Zhang, J. Chang, Y. Han, H. Li, Q. Luo, C.-Q. Ma, H.-L. Yip, L. Ding and J. Yang, *Cell Rep. Phys. Sci.*, 2024, **5**, 101883.

20 H. Hu, Z. Jin, J. Ge, C. Shen, L. Xie, W. Song, Q. Ye, P. Ding, J. Li, C. Han, X. Yu, Q. Liu and Z. Ge, *Adv. Mater.*, 2025, **37**, 2420308.

21 S. Park, S. Yoon, H. Ahn, H. Yu, E.-Y. Shin, K. Cho, Y. H. Jang, Y. Jun and H. J. Son, *Joule*, 2025, **9**, 101927.

22 B. Zhang, W. Chen, H. Chen, G. Zeng, R. Zhang, H. Li, Y. Wang, X. Gu, W. Sun, H. Gu, F. Gao, Y. Li and Y. Li, *Energy Environ. Sci.*, 2024, **17**, 2935–2944.

23 Z. Jin, C. Shen, H. Hu, C. Han, Y. Bai, M. Yang, Q. Liu and Z. Ge, *Energy Environ. Sci.*, 2025, **18**, 5552–5563.
24 H. Gu, J. Zhu, H. Chen, G. Zeng, X. Chen, X. Tang, J. Xia, T. Zhang, B. Zhang, J. Zhang, J. Ding, Y. Li and Y. Li, *Giant*, 2024, **18**, 100286.
25 H. Mao, J. Zhang, L. Wen, L. Tan, Y. Liu, J. Yang, Z. Qin, L. Zhang, Y. Zhai and Y. Chen, *Adv. Mater.*, 2025, **37**, 2505266.
26 Y. Li, Z. Jia, P. Huang, T. Liu, D. Hu, Y. Li, H. Liu, X. Lu, S. Lu, X. Yin and Y. (Michael) Yang, *Adv. Energy Mater.*, 2024, **14**, 2304000.
27 Z. Jia, J. Pan, X. Chen, Y. Li, T. Liu, H. Zhu, J. Yao, B. Yan and Y. (Michael) Yang, *Energy Environ. Sci.*, 2024, **17**, 3908–3916.
28 J. Fan, Z. Liu, J. Rao, K. Yan, Z. Chen, Y. Ran, B. Yan, J. Yao, G. Lu, H. Zhu, C. Li and H. Chen, *Adv. Mater.*, 2022, **34**, 2110569.
29 Y. Jiang, X. Dong, L. Sun, T. Liu, F. Qin, C. Xie, P. Jiang, L. Hu, X. Lu, X. Zhou, W. Meng, N. Li, C. J. Brabec and Y. Zhou, *Nat. Energy*, 2022, **7**, 352–359.
30 S. Dong, T. Jia, K. Zhang, J. Jing and F. Huang, *Joule*, 2020, **4**, 2004–2016.
31 H. Chen, R. Zhang, X. Chen, G. Zeng, L. Kobera, S. Abbrent, B. Zhang, W. Chen, G. Xu, J. Oh, S.-H. Kang, S. Chen, C. Yang, J. Brus, J. Hou, F. Gao, Y. Li and Y. Li, *Nat. Energy*, 2021, **6**, 1045–1053.
32 X. Dong, Y. Jiang, L. Sun, F. Qin, X. Zhou, X. Lu, W. Wang and Y. Zhou, *Adv. Funct. Mater.*, 2022, **32**, 2110209.
33 J. Xiang, Z. Liu, H. Chen and C. Li, *Adv. Mater.*, 2023, **35**, 2303729.
34 T. Chen, X. Zheng, D. Wang, Y. Zhu, Y. Ouyang, J. Xue, M. Wang, S. Wang, W. Ma, C. Zhang, Z. Ma, S. Li, L. Zuo and H. Chen, *Adv. Mater.*, 2024, **36**, 2308061.
35 R. Sun, T. Wang, X. Yang, Y. Wu, Y. Wang, Q. Wu, M. Zhang, C. J. Brabec, Y. Li and J. Min, *Nat. Energy*, 2022, **7**, 1087–1099.
36 J. Wang, Y. Wang, K. Xian, J. Qiao, Z. Chen, P. Bi, T. Zhang, Z. Zheng, X. Hao, L. Ye, S. Zhang and J. Hou, *Adv. Mater.*, 2024, **36**, 2305424.
37 J. Wang, Y. Wang, P. Bi, Z. Chen, J. Qiao, J. Li, W. Wang, Z. Zheng, S. Zhang, X. Hao and J. Hou, *Adv. Mater.*, 2023, **35**, 2301583.
38 L. Zhu, M. Zhang, G. Zhou, Z. Wang, W. Zhong, J. Zhuang, Z. Zhou, X. Gao, L. Kan, B. Hao, F. Han, R. Zeng, X. Xue, S. Xu, H. Jing, B. Xiao, H. Zhu, Y. Zhang and F. Liu, *Joule*, 2024, **8**, 3153–3168.
39 J. Wang, Y. Wang, M. Du, Y. Yu, C. Wang, W. Wang, Q. Guo, Y. Cui, S. Zhang and J. Hou, *Energy Environ. Sci.*, 2024, **17**, 8368–8378.
40 Z. Li, L. Zhan, H. Qiu, X. Sun, H. Hu, R. Gui, H. Yin, R. Sun, J. Min, J. Yu, W. Fu, W. Qiu, Z.-X. Liu, S. Yin and H. Chen, *Energy Environ. Sci.*, 2024, **17**, 8293–8303.
41 R. Basu, F. Gumpert, J. Lohbreier, P.-O. Morin, V. Vohra, Y. Liu, Y. Zhou, C. J. Brabec, H.-J. Egelhaaf and A. Distler, *Joule*, 2024, **8**, 970–978.
42 E. Feng, C. Zhang, J. Chang, F. Zhao, B. Hu, Y. Han, M. Sha, H. Li, X.-J. Du, C. Long, Y. Ding, Z.-J. Yang, H. Yin, Q. Luo, C.-Q. Ma, G. Lu, Z. Ma, X.-T. Hao and J. Yang, *ACS Nano*, 2024, **18**, 28026–28037.
43 B. Kim, Y. Lee, D. Um, W. Jeong, S. Lee, K. Kim, G. Nam, H. Hwang, S. Kim, T. Kim, K. Lee, H. Kang and B. Kim, *Adv. Funct. Mater.*, 2024, **34**, 2407403.
44 H. Chen, W. Sun, R. Zhang, Y. Huang, B. Zhang, G. Zeng, J. Ding, W. Chen, F. Gao, Y. Li and Y. Li, *Adv. Mater.*, 2024, **36**, 2402350.

45 F. Qin, L. Sun, H. Chen, Y. Liu, X. Lu, W. Wang, T. Liu, X. Dong, P. Jiang, Y. Jiang, L. Wang and Y. Zhou, *Adv. Mater.*, 2021, **33**, 2103017.
46 E. Jayaraman, M. Prete, A. Chandel, F. Faseela, K. Wang, C. Y. Ho, J. Lamminaho and M. Madsen, *Adv. Energy Mater.*, 2025, e04465.
47 Y. Shen, H. Zhang, J. Zhang, C. Tian, Y. Shi, D. Qiu, Z. Zhang, K. Lu and Z. Wei, *Adv. Mater.*, 2023, **35**, 2209030.
48 C. Tian, J. Zhang, Y. Shen, H. Zhang, Z. Zhang, D. Qiu, L. Zhang and Z. Wei, *Solar RRL*, 2023, **7**, 2300349.
49 Y. Liu, F. Qin, Y. Wang, X. Lu, Z. Xiong, C. Xie and Y. Zhou, *Adv. Funct. Mater.*, 2024, **34**, 2408453.
50 S. Yang, X. Chen, Y. Pan, J. Fang, Y. Han, Z. Wang, F. Qian, W. Qi, K. Shui, Q. Zhang, F. Guo, Y. Sun, C. Ma and Q. Luo, *Adv. Mater.*, 2025, **37**, 2500115.
51 X. Lu, C. Xie, Y. Liu, H. Zheng, K. Feng, Z. Xiong, W. Wei and Y. Zhou, *Nat. Energy*, 2024, **9**, 793–802.
52 C. Xie, Z. Xiong, X. Liu, W. Wang, Y. Liu, X. Jiang, X. Lu, L. Sun and Y. Zhou, *Sci. China Chem.*, 2025, **68**, 1199–1206.
53 Q. Zhou, J. Chen, X. Zhou, X. Liu, X. Lu, R. Wei, Y. Liu, Z. Zhang, Z. Xiong, S. Xiong and Y. Zhou, *J. Mater. Chem. A*, 2025, **13**, 3720–3726.
54 X. Lu, Y. Liu, R. Tian, X. Liu, Y. Wang and Y. Zhou, *Energy Environ. Sci.*, 2025, **18**, 2426–2435.
55 X. Zhou, X. Liu, X. Dong, T. Liu, K. Feng, Q. Luo, R. Tian, S. Xiong, L. Sun, J. Chen, Z. Zhang, R. Wei and Y. Zhou, *Adv. Funct. Mater.*, 2025, e07399.
56 K. Feng, X. Zhou, Y. Gao, J. Chen, J. Liu, X. Liu, Q. Luo, Q. Zhou, Z. Xiong, X. Wang, M. Shao, H. Han and Y. Zhou, *Angew. Chem., Int. Ed.*, 2025, **64**, e202420226.
57 H. Li, J. Le, H. Tan, L. Hu, X. Li, K. Zhang, S. Zeng, Q. Liu, M. Zhang, L. Shi, Z. Cai, S. Liu, H. Li, L. Ye, X. Hu and Y. Chen, *Adv. Mater.*, 2025, **37**, 2411989.